Fabrication of Fe Nanoparticle Assemblies on Au(111) with Xe Buffer Layer and Low Temperature Growth

Wen-Chin Lin, Huang-Yu Chang[1], Yu-Tsen Hu[1], and Chien-Cheng Kuo[1,2*]

Department of Physics, National Taiwan Normal University, Taipei 11677, Taiwan
[1]*Department of Physics, National Sun Yat-sen University, Kaohsiung 80424, Taiwan*
[2]*Center for Nanoscience and Nanotechnoloy, National Sun Yat-sen University, Kaohsiung 80424, Taiwan*

Received January 15, 2009; accepted May 20, 2009; published online August 20, 2009

Growth of Fe nanoparticle assemblies on Au(111) herringbone surface is systematically studied by scanning tunneling microscope (STM) through the variation of (1) deposition coverage, (2) substrate temperature, (3) Xe buffer layer assisted growth (BLAG), and (4) nucleation seed effect. 0.09–0.18 ML Fe deposited at 230–250 K results in regular nanoparticle arrays, which can serve as templates with well-ordered nucleation sites for subsequent growth. BLAG and 90 K growth lead to the multi-layer height nanoparticles. Combination of Xe buffer layer and nucleation seeds is demonstrated to be a new method for the nanoparticle growth on nano-patterned template, maintaining the three-dimensional shape and ordering without lateral percolation.

DOI: 10.1143/JJAP.48.08JB07

1. Introduction

In the last decade, nano-patterned templates attracted much attention because of the promising capability for the preparation of well-arranged nanodots.[1–6] For example, the dislocation network formed by 2 monolayer (ML) Ag on Pt(111) is a template for fabrication of well-ordered, two-dimensional nanocluster arrays.[2,7] While Au atoms are deposited onto N–Cu(100) surface with submonolayer coverage, nitrogen areas act as a mask for the growth of Au atoms, leading to a square lattice of Au islands with the inter-island distance ≈5 nm.[3,8] The regularly spaced corners of Au(111) herringbone surface are preferred nucleation sites for 3d transition metals, such as Fe, Co, Ni, and Mn.[1,4,9–14] Various vicinal surfaces, such as Pt(997) and Au(788), also provide regular steps for nucleation of nanostructures.[15–17] However, in all of these cases, while increasing coverage, the well-arranged nuclei generally grow as two-dimensional (2D) islands and then evolve into continous thin films. The natural limitation of 2D islands restricts the functions for the further applications, because three-dimensional (3D) nanoparticles are usually required to enhance either the catalytic capability or Curie temperature of long range magnetic ordering.[18] Besides, with buffer layer assisted growth (BLAG), the Fe nanoparticle size can be manipulated by properly choosing Xe thickness and Fe coverage.[19,20] In this report, BLAG and nucleation seeds on Au(111) herringbone surface are combined for fabrication of Fe nanoparticle assemblies. BLAG clearly changes the conventional single atomic height Fe islands (grown at 230–320 K) into 3D nanoparticles (height ≥2 atomic layers). Besides, the pre-deposited regular Fe nucleation seeds successfully attract the Fe nanoparticles, formed by BLAG, to assemble the regular Fe nanoparticle arrays. This new method of "BLAG on nano-patterned template" should be able to repeat further in order to enlarge the 3D nanopaticles. It is supposed to be a very useful method for the preparation of various supported 3D nanoparticles with regular spatial arrangement and controlled size.

2. Experimental Procedure

The experiment was performed in a multi-functional ultra high vacuum (UHV) chamber with base pressure batter than 4×10^{-11} mbar. All the sample preparation and characterization were carried out *in situ*. After cycles of 500 eV Ar^+ sputtering and annealing, Au(111) surface with herringbone structure was prepared. To grow Fe nanoparticles, Fe atoms evaporated by e-beam heating were deposited onto either the bare substrate or the substrate covered with Xe buffer layer. The deposition rate of Fe was 9×10^{-4} ML/s. Xe buffer layer assisted growth was performed by adsorption of Xe, and subsequent Fe deposition at 90 or 33 K. Then the sample was annealed to 300 K for the desorption of Xe and formation of Fe nanoparticles on the surface. The grown samples were characterized by an UHV-scanning tunneling microscope (STM) for further analysis.

3. Results and Discussion

3.1 Well-ordered Fe nucleations

The first question of this study is how to prepare the well-ordered Fe islands on Au(111) with few deposition coverage. STM characterization of Fe growth on Au(111) herringbone surface has been reported by several groups.[1,9,10] In Stroscio *et al.*'s study, nucleation of Fe islands was observed to occur at the corners of the herringbone reconstruction.[1] Initial Fe growth proceeds in a nonideal layer-by-layer growth mode. New layers start before preceding layers are nearly complete. Khan *et al.*'s report reveals initial growth of Fe on Au(111) at 323 K.[10] At 0.08 ML Fe, the particles appear round with some sharp edges. At 0.28 ML Fe, the particles are more uniform in size and appear triangular. Nevertheless, the preparation of well-ordered Fe islands on Au(111) is crucial and still lacking for systematic studies. It is strongly dependent on the deposition coverage and growth (substrate) temperature.

Figure 1 shows STM images of Fe grown on Au(111) with the variation of Fe coverage and growth temperature. The statistical normalized nucleation densities (normalized by the density of herringbone corners) for various growth conditions are summarized in Table I. For 0.02–0.05 ML Fe grown at 300–320 K, the nucleations are randomly distributed with the densities ~48–67%. From the comparison between Figs. 1(a) and 1(b), higher Fe coverage certainly increases the normalized nucleation density. From

*E-mail address: cckuo@faculty.nsysu.edu.tw

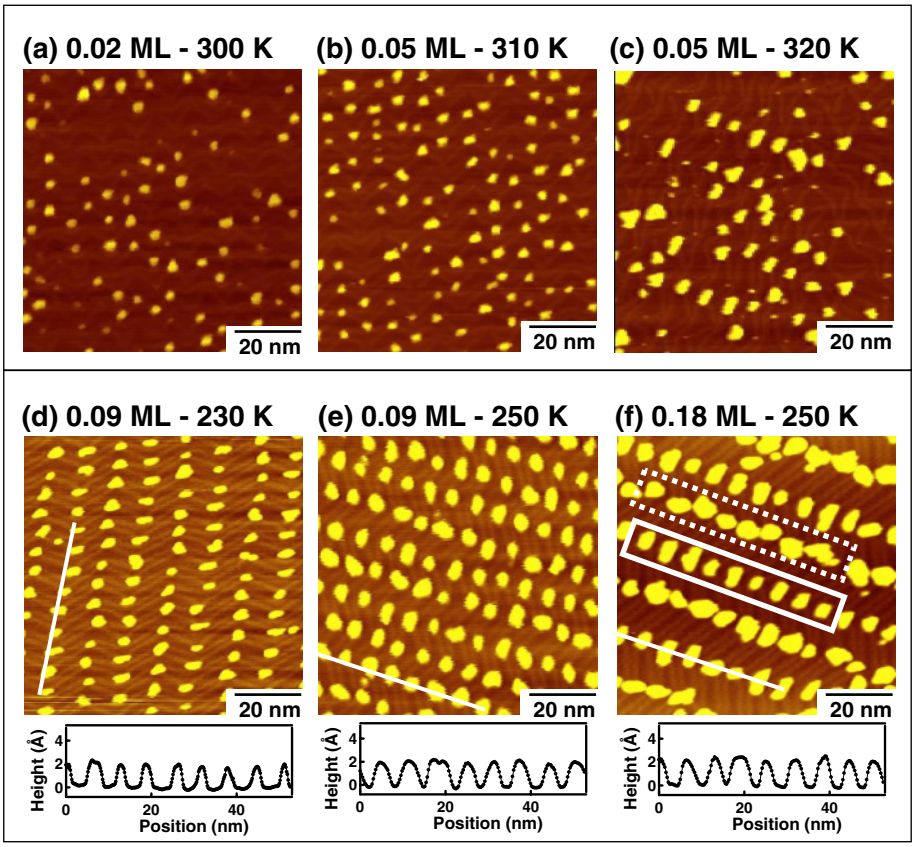

Fig. 1. (Color online) STM images of Fe deposition on Au(111) at various growth temperature. In (d)–(f), 0.09–0.18 ML Fe deposited at 230–250 K results in the regular nanoparticle arrays. The insets reveal the line profiles, indicating the single atomic height of the Fe nanoparticles. The rectangles of solid and dotted lines indicate fcc and hcp herringbone corners.

Table I. Normalized nucleation densities (by density of herringbone corners) of 0.02–0.18 ML Fe/Au(111) grown at 230–320 K.

Fe coverage (ML)	Growth temperature (K)	Nucleation density (%)
0.02	300	48 ± 2
0.05	310	67 ± 5
0.05	320	56 ± 2
0.09	230	101 ± 2
0.09	250	100 ± 2
0.18	250	105 ± 2

Figs. 1(b) and 1(c), higher growth temperature might increase the mobility of Fe atoms for crossing the herringbone structure. Thus the normalized nucleation density clearly decreases for 320 K growth. In the growth of 0.1 ML Ag nanoparticles on the 2 ML Ag/Pt(111) nano-patterned template, the particle density saturates the network unit cell while the growth temperature = 100–130 K.[2] For growth temperature above 140 K, the particle density decreases and the arrangement becomes disordered. Therefore, in comparison with the Ag/Pt(111) template, the confinement barrier height of Au(111) herringbone surface is higher and the particle array should be more stable.

In Figs. 1(d)–1(f), the Fe nucleation islands saturate all the corners of herringbone reconstruction. The variations of 0.09–0.18 ML and 230–250 K seem insignificant for the preparation of well-ordered Fe nucleation arrays. The line profiles indicate all the islands are of one atomic height. For 0.18 ML Fe at 250 K, some irregular islands (~5%) appear out of the herringbone corners. Interestingly, in Fig. 1(f), there are quite different characters for the nucleation islands at different herringbone corners. Actually the Au(111) herringbone structure is composed of face-center cubic (fcc) and hexagonal close-packed (hcp) zigzag domains. The fcc and hcp corners, as indicated by rectangles of solid and dotted lines in Fig. 1(f), are the preferred Fe nucleation sites. Apparently Fe islands are of different shape and size in different corners. Fcc corners prefer to form rectangular shape and smaller size of Fe islands, while hcp corners prefer round shape and larger size. It is probably due to the variation of local crystalline structure in different corners and the resultant variation of lattice mismatch or stress in the Fe islands.

3.2 Xe BLAG

Xe BLAG has been extensively used for the preparation of nanoparticle assemblies in recently years.[19] The advantage of BLAG is the feasibility for numerous materials of nanoparticles on various substrates. In this study, Xe buffer layers are adsorbed at either 90 or 33 K and then subsequently desorbed during 300 K annealing. In Fig. 2, STM images of (a) 0.09 ML and (b) 0.18 ML Fe on Au(111) with 4 L Xe buffer layer assisted growth, as well as the histograms are shown. For 0.09 ML Fe/4 L Xe, only single atomic height particles can be seen, while for 0.18 ML Fe/4 L Xe, particles with 2 ML height are

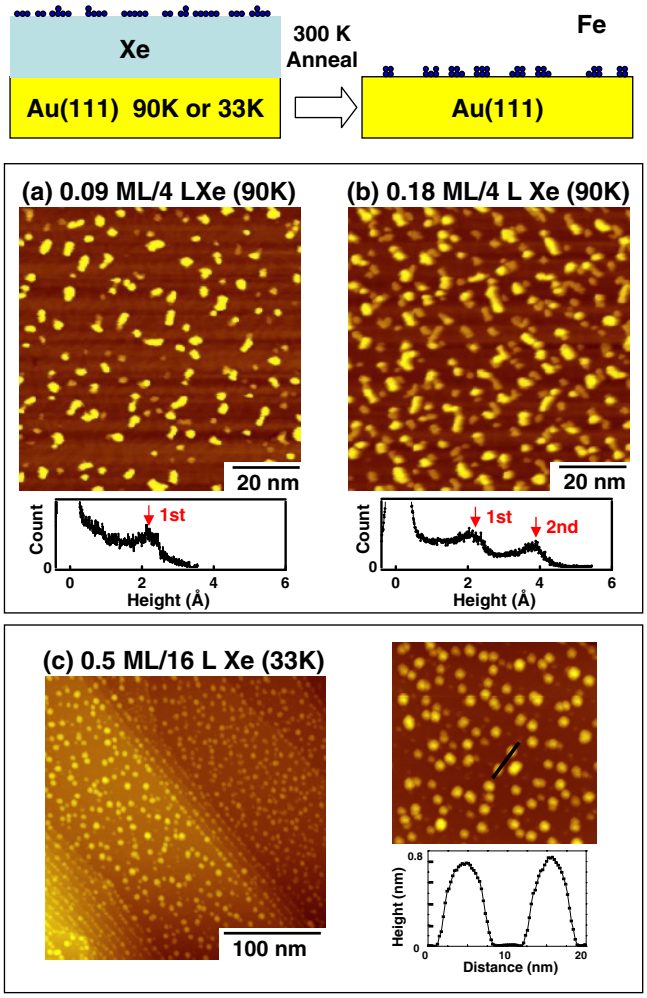

Fig. 2. (Color online) STM images of (a) 0.09 ML and (b) 0.18 ML Fe on Au(111) with 4 L Xe buffer layer adsorbed at 90 K. (c) is 0.5 ML Fe/Au(111) with 16 L Xe adsorbed at 33 K. The growth processes are exhibited in the upper panel. The height histograms of each STM images are shown below the images. For 0.09 ML Fe/4 L Xe, only single atomic height particles can be seen, while for 0.18 ML Fe/4 L Xe, particles with 2 atomic height are frequently observed. In (c), with higher Fe and Xe coverage, nanoparticle assemblies of 3–4 atomic height are prepared.

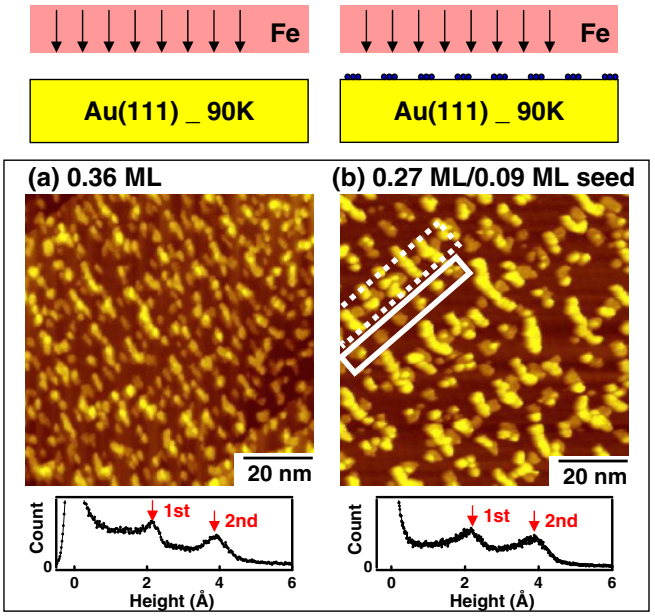

Fig. 3. (Color online) STM images of (a) 0.36 ML Fe deposited on Au(111) at 90 K, and (b) 0.27 ML Fe deposited at 90 K on seeded surface prepared by depositing 0.09 ML Fe on Au(111) at 250 K. The growth processes are exhibited in the upper panel. The histograms of each STM images are revealed, indicating the appearance of bi-layer height nanoparticles. The rectangles of solid and dotted lines indicate fcc and hcp corner rows, respectively.

frequently observed. Unlike the single atomic height islands in 250 K growth [Fig. 1(f)], the STM image in Fig. 2(b) surely reveal the enhanced formation of 3D islands. Further refinement of Fe coverage and Xe buffer layer thickness can change the size and shape of Fe particles even more, as shown in Fig. 2(c). For 0.5 ML Fe/Au(111) with 16 L Xe adsorbed at 33 K, nanoparticle assemblies of 3–4 atomic height are prepared. The subsequent studies in the rest of this report, such as combination of BLAG and nucleation seeds [comparison between Figs. 3(b) and 4(b)], also indicate the significant effect of Xe buffer layer.

3.3 Nucleation seed effect

Figure 3 shows the nucleation seed effect for the growth of Fe nanoparticles. For comparison, in Fig. 3(a), 0.36 ML of Fe is directly deposited on Au(111) at 90 K. In Fig. 3(b), seeds are prepared by depositing 0.09 ML Fe on Au(111) at 250 K, like that shown in Fig. 1(e). Then 0.18 ML Fe is deposited when the substrate temperature is 90 K. From the histograms, the two methods of Figs. 3(a) and 3(b) both result in multi-layer islands. Direct deposition at 90 K creates many disordered small islands. However one can clearly observe that proper seeding leads to more ordered Fe islands with larger size. Similar to Fig. 1(f), fcc and hcp herringbone corners reveal very different characteristics for the Fe island growth. For fcc corners, the islands tend to remain small, while close to hcp corners, the islands tend to attract larger amount of Fe atoms, forming big and elongated islands.

3.4 Combination of BLAG and nucleation seeds

Finally, Xe-buffer layer and nucleation seeds are combined for the preparation of Fe nanoparticle assemblies. Nucleation seeds are prepared on Au(111), like Figs. 1(b) and 1(e), for the sequential growth shown in Figs. 4(a) and 4(b), respectively. 8 L Xe buffer layer is adsorbed on the template, and then Fe deposition is carried out, both at 90 K. Subsequent annealing up to 300 K causes the Xe desorption. During Xe desorption, Fe atoms gradually aggregate to form nanoparticles on the surface. One interesting question is whether the Fe nanoparticles will preferentially land on the positions of nucleation seeds. The results are exhibited in Figs. 4(a) and 4(b) with 0.05 and 0.09 ML Fe nucleation seeds, respectively. The line profiles and histograms are revealed, indicating the 2-layer height nanoparticles. Rectangular lattice is shown for the reference of the regular particle arrays. For Fig. 4(a), since the 0.05 ML Fe nucleation seeds do not fully saturate all of the herringbone corner [cf. Fig. 1(b)], the order of Fe nanoparticles is discernible, but not very distinct. For Fig. 4(b), since the 0.09 ML Fe nucleation seeds do fully saturate all of the herringbone

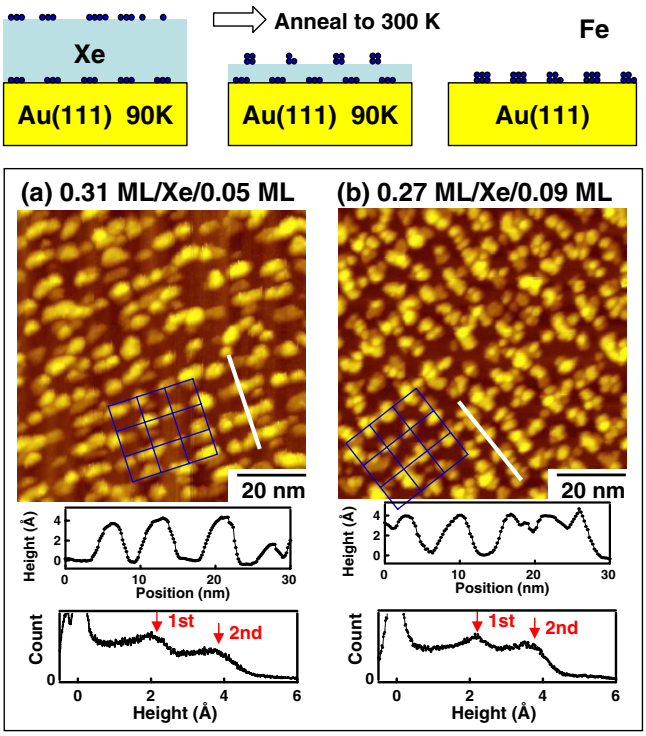

Fig. 4. (Color online) STM images for the combination of nucleation seed effect, and buffer layer assisted growth with 8 L Xe adsorbed at 90 K. The growth processes are exhibited in the upper panel. The line profiles and histograms are shown, indicating the bi-layer height nanoparticles. Rectangular lattice is shown for the reference of the regular particle arrays.

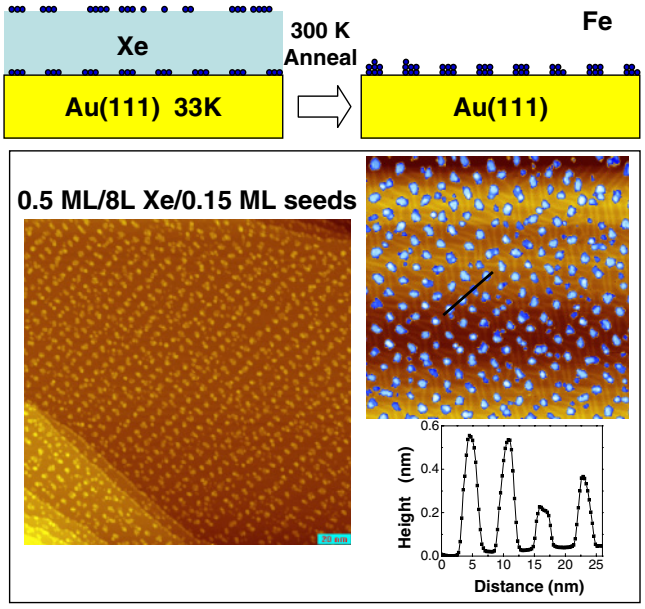

Fig. 5. (Color online) STM images for the combination of nucleation seed effect, and buffer layer assisted growth with 8 L Xe adsorbed at 33 K. The growth processes are exhibited in the upper panel. The line profiles indicates the multi-layer height nanoparticles.

corners [cf. Fig. 1(e)], the order of Fe nanoparticles is obvious to observe.

Figure 5 is the experimental result of 0.5 ML Fe/8 L Xe adsorbed at 33 K/0.15 ML Fe seeds/Au(111). The regular ordering of Fe nanoparticles is clearly observed. As indicated in the line profile, the particle height accumulates up to 2–3 atomic height without lateral expanding. The pre-deposited regular Fe nucleation seeds are preferential sites for the Fe nanoparticles formed by BLAG to nucleate, leading to the regular 3D Fe nanoparticle arrays.

The combination of BLAG and nucleation seeds associates the advantages of 3D nanoparticle growth and regular spatial arrangement, as exhibited in Figs. 4 and 5. Nevertheless, the detailed physical mechanism is still not fully understood. For example, why do the subsequently formed nanoparticles (by BLAG) prefer to nucleate on the pre-deposited seeds? Actually, while looking into the details, the growth results of Figs. 4 and 5 are quite different. The thickness of Xe buffer layer is supposed to be one of the key factors. Basically, the Xe buffer layer has two kinds of effects on the Fe nanoparticle formation. First, even only submonolayer Xe on the surface might help Fe atoms or nanoparticles to diffuse more quickly and easily toward the most stable sites, the herringbone corners. The results shown in Fig. 4 are of this case. In previous studies, most of Xe desorbs before 90 K.[21] Thus only submonolayer Xe is supposed to be trapped on the herringbone surface at 90 K, and changes the Fe diffusion mode to form the results of Fig. 4. In the condition of thick Xe layer, for example adsorption at 33 K, Fe atoms gradually diffuse into the Xe layer, toward the herringbone surface, while annealing to room temperature. The thicker Xe layer provides more time and longer penetration length for Fe atoms to aggregate as larger nanoparticles before arriving Au(111) herringbone surface. Results of Figs. 2(c) and 5 are of this case. While most of Xe already desorbs, the residual Xe on the surface might also promote the diffusion of Fe nanoparticles toward the seeded corners, instead of being trapped at random position. The authors need to agree that the above discussion is just one of the possibilities. For the more convincing and more detailed explanation of growth mechanism, one might need to perform STM imaging during the Xe desorption processes, which is really worth studying, but out of the scope of this report.

4. Conclusions

In summary, growth of Fe nanoparticles on Au(111) herringbone reconstruction is systematically studied by STM with the variation of growth parameters. 0.09–0.18 ML Fe deposited at 230–250 K leads to ordered nanoparticle arrays, providing well-ordered nucleation seeds for the subsequent Fe deposition. Xe buffer layer and low temperature (90 K) deposition result in nanoparticles with multi-layer height. The method of "BLAG on nano-patterned template" is shown to be a useful method for the preparation of various supported 3D nanoparticles with regular spatial arrangement and controlled size.

Acknowledgments

The authors thank Dr. Ker-Jar Song for the constructive discussion. This work was supported by the National Science Council of Taiwan under Grant Nos. NSC 96-2112-M-003-015-MY3, NSC 96-2112-M-110-002, and NSC 97-2112-M-110-003-MY3.

1) J. A. Stroscio, D. T. Pierce, R. A. Dragoset, and P. N. First: J. Vac. Sci. Technol. A **10** (1992) 1981.
2) K. Bromann, M. Giovannini, H. Brune, and K. Kern: Eur. Phys. J. D **9** (1999) 25.
3) F. Leibsle, S. S. Dhesi, S. Barrett, and A. Robinson: Surf. Sci. **317** (1994) 309.
4) B. Voigtländer, G. Meyer, and N. Amer: Phys. Rev. B **44** (1991) 10354.
5) W. C. Lin, C. C. Kuo, M. F. Luo, K. J. Song, and M.-T. Lin: Appl. Phys. Lett. **86** (2005) 043105.
6) M. F. Luo, C. I. Chiang, H. W. Shiu, S. D. Sartale, and C. C. Kuo: Nanotechnology **17** (2006) 360.
7) H. Brune, M. Giovannini, K. Bromann, and K. Kern: Nature **394** (1998) 451.
8) H. Ellmer, V. Repain, M. Sotto, and S. Rousset: Surf. Sci. **511** (2002) 183.
9) J. Meyer, I. Baikie, E. Kopatzki, and R. Behm: Surf. Sci. **365** (1996) L647.
10) N. A. Khan and C. Matranga: Surf. Sci. **602** (2008) 932.
11) D. T. Dekadjevi, B. J. Hickey, and S. Brown: Phys. Rev. B **71** (2005) 054108.
12) P. Ohresser, N. B. Brookes, S. Padovani, F. Scheurer, and H. Bulou: Phys. Rev. B **64** (2001) 104429.
13) H. Bulou, F. Scheurer, P. Ohresser, A. Barbier, S. Stanescu, and C. Quiros: Phys. Rev. B **69** (2004) 155413.
14) S. Padovani, F. Scheurer, and J. Bucher: Europhys. Lett. **45** (1999) 327.
15) V. Repain, G. Baudot, H. Ellmer, and S. Rousset: Europhys. Lett. **58** (2002) 730.
16) V. Repain, S. Rohart, Y. Girard, A. Tejeda, and S. Rousset: J. Phys.: Condens. Matter **18** (2006) S17.
17) P. Gambardella, M. Blanc, L. Bürgi, K. Kuhnke, and K. Kern: Surf. Sci. **449** (2000) 93.
18) W. C. Lin, P. C. Huang, K. J. Song, and M.-T. Lin: Appl. Phys. Lett. **88** (2006) 153117.
19) R. Skomski, J. Zhang, V. Sessi, J. Honolka, K. Kern, and A. Enders: J. Appl. Phys. **103** (2008) 07D519.
20) W. C. Lin, S. S. Wong, P. C. Huang, C. B. Wu, B. R. Xu, C. T. Chiang, H. Y. Yen, and M.-T. Lin: Appl. Phys. Lett. **89** (2006) 153111.
21) C. Wang and R. Gomer: Surf. Sci. **91** (1980) 533.